



## PAPER

## Microdosimetric calculations of the direct DNA damage induced by low energy electrons using the Geant4-DNA Monte Carlo code

Stefanos Margis<sup>1</sup>, Maria Magouni<sup>1</sup>, Ioanna Kyriakou<sup>1</sup>, Alexandros G Georgakilas<sup>2</sup>, Sebastien Incerti<sup>3,4</sup> and Dimitris Emfietzoglou<sup>1,5</sup><sup>1</sup> Medical Physics Laboratory, University of Ioannina Medical School, 45110 Ioannina, Greece<sup>2</sup> DNA Damage Laboratory, Physics Department, School of Applied Mathematical and Physical Sciences, National Technical University of Athens (NTUA), Zografou, Athens, Greece<sup>3</sup> University of Bordeaux, CENBG, UMR 5797, F-33170 Gradignan, France<sup>4</sup> CNRS, IN2P3, CENBG, UMR 5797, F-33170 Gradignan, France<sup>5</sup> Author to whom any correspondence should be addressed.E-mail: [demfietz@uoi.gr](mailto:demfietz@uoi.gr) and [demfietz@gmail.com](mailto:demfietz@gmail.com)**Keywords:** Geant4-DNA, microdosimetry, DNA damageRECEIVED  
8 November 2019REVISED  
4 January 2020ACCEPTED FOR PUBLICATION  
14 January 2020PUBLISHED  
12 February 2020**Abstract**

To calculate the yield of direct DNA damage induced by low energy electrons using Monte Carlo generated microdosimetric spectra at the nanometer scale and examine the influence of various simulation inputs. The potential of classical microdosimetry to offer a viable and simpler alternative to more elaborate mechanistic approaches for practical applications is discussed. Track-structure simulations with the Geant4-DNA low-energy extension of the Geant4 Monte Carlo toolkit were used for calculating lineal energy spectra in spherical volumes with dimensions relevant to double-strand-break (DSB) induction. The microdosimetric spectra were then used to calculate the yield of simple and clustered DSB based on literature values of the threshold energy of DNA damage. The influence of the different implementations of the dielectric function of liquid water available in Geant4-DNA (Option 2 and Option 4 constructors), as well as the effect of particle tracking cutoff energy and target size are examined.

Frequency- and dose-mean lineal energies in liquid-water spheres of 2, 2.3, 2.6, and 3.4 nm diameter, as well as, number of simple and clustered DSB/Gy/cell are presented for electrons over the 100 eV to 100 keV energy range. Results are presented for both the ‘default’ (Option 2) and ‘Ioannina’ (Option 4) physics models of Geant4-DNA applying several commonly used tracking cutoff energies (10, 20, 50, 100 eV). Overall, the choice of the physics model and target diameter has a moderate effect (up to ~10%–30%) on the DSB yield whereas the effect of the tracking cutoff energy may be significant (>100%). Importantly, the yield of both simple and clustered DSB was found to vary significantly (by a factor of 2 or more) with electron energy over the examined range.

The yields of electron-induced simple and clustered DSB exhibit a strong energy dependence over the 100 eV–100 keV range with implications to radiation quality issues. It is shown that a classical microdosimetry approach for the calculation of DNA damage based on lineal energy spectra in nanometer-size targets predicts comparable results to computationally intensive mechanistic approaches which use detailed atomistic DNA geometries, thus, offering a relatively simple and robust alternative for some practical applications.

**1. Introduction**

Microdosimetry is useful for investigating radiation quality issues when the relative biological effectiveness (RBE) cannot be deduced directly (ICRU 1983, ICRU 1986). It is widely accepted that the nuclear DNA is one of the most important cellular targets for the biological effects of ionizing radiation (Goodhead 1989, Georgakilas *et al* 2013, Nikjoo *et al* 2016b, Schuemann *et al* 2019a). However, experimental measurements of the yield of the various forms of radiation-induced DNA damage, especially of the clustered form, are challenging (Falk *et al*

2010, Nikitaki *et al* 2016). The Monte Carlo (MC) technique, which enables stochastic simulation of radiation tracks in matter, offers an important theoretical tool for quantifying DNA damage induced by different radiation qualities (Hill 1999, Semenenko and Stewart 2004, Bernal and Liendo 2009, Alloni *et al* 2012, Pater *et al* 2014, Nikjoo *et al* 2016b, Friedland *et al* 2017, McNamara *et al* 2017, Chatzipapas *et al* 2019, Henthorn *et al* 2018, Liu *et al* 2018, Schuemann *et al* 2019b). The results of such studies depend, mainly, on the physics models used in the MC simulation and the geometrical model used to represent the DNA target. At a more sophisticated level, additional models are included to simulate the chemical stage of radiation action (indirect effect) and the DNA damage/repair processes (Friedland *et al* 2011, Taleei and Nikjoo 2012, Meylan *et al* 2017, Henthorn *et al* 2018, Ramos-Mendez *et al* 2018, Ingram *et al* 2019).

The physics models for MC radiation transport simulations are broadly classified as condensed-history (CH) or track-structure (TS) (Andreo 1991, Nikjoo *et al* 2006). In CH models charged-particle transport is simulated via artificial steps (much longer than the mean free path) using multiple-scattering theories (Nahum 1999, Salvat and Fernández-Varea 2009). Thus, the track of the charged particle is ‘condensed’ to fewer simulation steps and energy-loss is assumed to be ‘continuous’ along those steps. As a result, CH models offer a huge reduction in simulation time at the expense of inferior spatial resolution which, in general, is on the order of 0.1–1 mm (Dingfelder 2012, Lazarakis *et al* 2018). In addition, the use of multiple-scattering theories makes CH models most accurate for high-energy charged particles; typically in the MeV energy range. CH models comprise the main physics input of the so-called general-purpose MC codes, such as MCNP (Goorley *et al* 2016), EGS (Kawrakow 2000), GEANT4 (Agostinelli *et al* 2003, Allison *et al* 2006, 2016), FLUKA (Ferrari *et al* 2005), and PENELOPE (Baró *et al* 1995). On the other hand, TS models enable the simulation of radiation tracks in a ‘discrete’ manner, interaction-by-interaction, based on single-scattering cross sections. In principle, TS models can be extended down to very low energies (eV scale) offering superior spatial resolution which may reach the nanometer scale (Dingfelder 2006, Emfietzoglou *et al* 2017a). Although most present day general-purpose codes (see above) enable simulation of hard collisions (i.e. those with large energy- or momentum-transfer) in a discrete manner, the treatment of the remaining (soft) collisions by CH models, limits their validity to electron transport above ~0.1–1 keV.

It follows from the above discussion that TS models are much better suited for microdosimetry at the sub-cellular and DNA level compared to CH models. The main drawback of TS models is that they are computer intensive so they are generally limited to low-medium energy charged particles (e.g. typically to electrons below ~100 keV). In addition, TS models are far more uncertain, since in the eV–keV energy range, interaction cross sections become very sensitive to the electronic band structure of the material (Dingfelder *et al* 1998, Champion 2003, Dingfelder 2006, Emfietzoglou *et al* 2012, 2017b, Garcia-Molina *et al* 2017) while the underlying assumption of well-defined electron trajectories may also be questioned (Thomson and Kawrakow 2011, 2018, Liljequist and Nikjoo 2014). Among more than a dozen TS codes (partly reviewed in Nikjoo *et al* (2006)), PARTRAC (Friedland *et al* 1998, 2011, Dingfelder *et al* 2008) and KURBUC (Liamsuwan *et al* 2012, Nikjoo *et al* 2016a) are perhaps the most known, and include elaborate models of sub-cellular structures as well as explicit DNA damage and repair pathways (Friedland *et al* 2011, Taleei and Nikjoo 2012). Results of TS simulations have been imported in a parameterized form to the fast Monte Carlo Damage Simulation (MCDS) software (Semenenko and Stewart 2004, 2006) to carry out fast DNA damage calculations for various applications (El Naqa *et al* 2012, Streitmatter *et al* 2017, Stewart *et al* 2015, 2018).

Since 2007 Geant4 version 9.1 offers a set of TS models for liquid water through the Geant4-DNA low-energy extension (Incerti *et al* 2010a, 2018, Bernal *et al* 2015). The Geant4-DNA package is also the transport engine behind the TOPAS-nBio MC code (Schuemann *et al* 2019a). Contrary to the Livermore and Penelope low-energy CH models of Geant4, which are based on atomic (and gas-phase) cross sections and have a recommended electron transport threshold of 250 eV and 100 eV, respectively, the TS models included in the Geant4-DNA package offer ionization and excitation cross sections specific to the liquid phase of water and allow full slowing-down simulations of electron tracks down to ~10 eV (Bernal *et al* 2015, Incerti *et al* 2018). The performance of the CH and TS models of Geant4 for micro- and nano-dosimetry has been recently investigated in several studies which reveal important differences at the nano-scale (Incerti *et al* 2016, 2019, Famulari *et al* 2017, Kyriakou *et al* 2017, 2019, Lazarakis *et al* 2018).

Geometrical models of DNA used in MC simulations vary significantly in terms of complexity. In general, we can distinguish between *amorphous* (structureless) DNA models that use nanometer-size spherical or cylindrical volumes to represent critical dimensions of the DNA target as a whole, and *atomistic* DNA models which account for the 3D geometry and explicit molecular structure of the DNA (e.g. the sugar-phosphate backbone and the individual DNA base-pairs) (Friedland *et al* 2008, Nikjoo and Girard 2012, McNamara *et al* 2018).

The ‘amorphous’ DNA models are commonly used in the context of *classical* or *regional* microdosimetry (ICRU 1983, Rossi and Zaider 1996). In this approach, stochastic quantities like the specific or lineal energy are calculated by MC simulation in nano- or micro-meter size spherical (or cylindrical) targets and then correlated to DNA damage empirically via consideration of the threshold energy of damage induction (Nikjoo *et al* 2002, 2011). A biophysical foundation for the microdosimetric approach is offered by the Theory of Dual Radiation Action

(TDRA) (Kellerer and Rossi 1974, 1978). Specifically, in the ‘site’ version of the TDRA, where the ‘interaction’ probability between pairs of sublesions is independent of their separation distance, the biological effectiveness (i.e. radiation quality) becomes proportional to the integral of the physical (radiation) and geometrical (target) proximity functions. This integral exactly equals the dose-weighted specific (or lineal) energy of the target (Rossi and Zaider 1996). Thus, the ‘site’ version of TDRA offers the biophysical framework for linking microdosimetric spectra to biological damage and, eventually, to radiation quality. Due to its computational simplicity and robustness, classical (or regional) microdosimetry is usually the method of choice for theoretical calculations of the relative biological effectiveness (RBE) of clinical beams/sources (Wuu *et al* 1996, Lindborg and Grindborg 1997, Wu and Zaider 1998, Taschereau *et al* 2003, Lindborg and Nikjoo 2011, Lindborg *et al* 2013, Famulari *et al* 2018). It also forms the basis of the microdosimetric-kinetic-model (MKM) which is used clinically in carbon ion treatment planning systems (Inaniwa *et al* 2010, Bopp *et al* 2016). Microdosimetry has been recognized as providing the physical basis for the definition of the quality factor (Q) in radiation protection (ICRU 1983, ICRU 1986).

The atomistic DNA models, on the other hand, are linked to the *mechanistic* approach of DNA damage which attempts to account for the ‘complete-chain’, i.e. the physical, chemical, and biological stages of radiation action (Nikjoo *et al* 2016b). Despite its sophistication, the mechanistic approach is far less practical because it requires huge computer resources and incorporates a large number of adjustable (and mostly unknown) parameters (Zaider *et al* 1994, Nikjoo *et al* 2016a, Friedland *et al* 2017, Lampe *et al* 2018a, 2018b, Sakata *et al* 2019).

It is worth noting that in both the microdosimetric and mechanistic approach a homogeneous liquid water medium is commonly used as a surrogate to the biological medium since it is the dominant constituent of cells (~70% by weight).

In the present work, we compare two physics models of Geant4-DNA, namely, the so-called ‘default’ model or Option 2 constructor and the ‘Ioannina’ model or Option 4 constructor, which employ different implementations of the dielectric function of liquid water for calculating ionization and excitation cross sections. It should be noted that the current high-energy limits in the two constructors are different, with Opt2 extending up to 1 MeV and Opt4 limited up to 10 keV. Lineal energy spectra of low energy electrons (100 eV–100 keV) in DNA-size volumes are calculated. The microdosimetric spectra are then used to estimate the yield of simple and clustered DNA damage (per Gy and per cell). Low energy electrons are encountered in various therapeutic (e.g. Auger-emitters, low-energy brachytherapy sources) and imaging (e.g. mammography soft x-rays) modalities and have been implicated to the observed increase of RBE for low-energy photon beams/sources (Nikjoo and Lindborg 2010, Stewart *et al* 2015, Streitmatter *et al* 2017). Specific aims of the work include: (i) to examine whether the more recent implementation of the dielectric function of liquid water in Geant4-DNA (Ioannina models) influences the simulation of microdosimetric spectra and subsequent DNA damage calculations, (ii) to quantify the degree of which the microdosimetry based calculations of simple and clustered DSB are influenced by some user-defined parameters, such as, the size of the assumed target and the particle tracking cutoff energy, and (iii) to test whether the ‘classical’ microdosimetry approach for calculating DNA damage induction offers a practical alternative to more elaborate mechanistic approaches based on atomistic DNA models.

## 2. Materials and methods

### 2.1. Physics models

In any Geant4 application the user must specify a set of particle processes and physics models that are needed for the particular simulation (i.e. the so-called Physics List). A particle process corresponds to a particular type of physical interaction (e.g. ionization) and can be described by any of several available physics models. These models provide all the needed interaction cross sections (e.g. total, differential in scattering angle and/or energy transfer). To facilitate their use, Geant4 offers interface C++ classes, called ‘physics constructors’, which contain a list of processes and models for a variety of applications. Regarding the TS simulation of electrons in liquid water, Geant4 offers three sets of physics models, namely, the default Geant4-DNA models (Incerti *et al* 2010b) released in Geant4 version 9.1, the models developed at the University of Ioannina (hereafter the ‘Ioannina’ models) (Kyriakou *et al* 2015, 2016) which were released in Geant4 version 10.2, and the so-called CPA100 physics models released in Geant4 version 10.4 (Bordage *et al* 2016). These models are assembled into the G4EmDNAPhysics\_option2 (or Opt2), G4EmDNAPhysics\_option4 (or Opt4), and G4EmDNAPhysics\_option6 (or Opt6) physics constructors, respectively. A fundamental difference between the above constructors concerns the energy-loss models. Specifically, Opt2 and Opt4 use the dielectric function of liquid water in order to include condensed-phase effects in the excitation and ionization cross sections whereas Opt6 uses a hybrid model with ionization cross sections pertaining to the gas phase. The details of the different implementation of the dielectric function in Opt2 and Opt4 and their impact upon electron transport have been discussed in some detail elsewhere (Kyriakou *et al* 2015, 2016). Importantly, recent studies have shown that the effect of the different dielectric function implementations on DNA damage induction (Lampe *et al* 2018a) and ionization clustering (Villagrasa *et al* 2019) may be significant. The two physics constructor (Opt2 and Opt4) used in the present study are summarized in

**Table 1.** The Geant4-DNA constructors examined in the present work with the corresponding physics models specifically developed for electron TS simulations in liquid water medium.

G4EmDNAPhysics_option2 (default models)		
Constructor	Model class	Physics model
Ionization	G4DNABornIonizationModel	Emfietzoglou dielectric model (11 eV–1 MeV)
Excitation	G4DNABornExcitationModel	Emfietzoglou dielectric model (9 eV–1 MeV)
Elastic scattering	G4DNAChampionElasticModel	Partial Wave analysis (7.4 eV–1 MeV)
G4EmDNAPhysics_option4 (ioannina models)		
Constructor	Model class	Physics model
Ionization	G4DNAEmfietzoglouIonizationModel	Emfietzoglou–Kyriakou dielectric model (10 eV–10 keV)
Excitation	G4DNAEmfietzoglouExcitationModel	Emfietzoglou–Kyriakou dielectric model (8 eV–10 keV)
Elastic scattering	G4DNAUeharaScreenedRutherfordElasticModel	Screened Rutherford model (9 eV–10 keV)

table 1. Briefly, ionization and excitation cross sections in Opt2 (default models) and Opt4 (Ioannina models) are calculated from first-principles based on the plane wave Born approximation (PWBA). The target response is considered by a semi-empirical model of the dielectric function of liquid water,  $\varepsilon(E, q)$ , with  $E$  and  $q$  being the energy- and momentum-transfer, respectively. The model dielectric function enables to calculate the energy-loss-function (ELF), defined as the imaginary part of the inverse dielectric function,  $\text{ELF} = \text{Im} \left( \frac{-1}{\varepsilon(E, q)} \right)$ , which is the main input in the calculation of inelastic cross sections in the PWBA (see appendix). Since condensed-phase effects are in-built in the dielectric function, inelastic cross section calculations by the ELF are widely considered as the preferred approach for extending high-energy approximations (e.g. Bethe theory) to the sub-keV energies where such effects are pronounced (Emfietzoglou and Nikjoo 2005, 2007). Note that the ELF is not only different for each material but also for the same material in different phases (e.g. gaseous versus liquid water).

The principal difference between Opt2 (default models) and Opt 4 (Ioannina models) is on the partitioning of the ELF to the different ionization shells and excitation levels of liquid water (see appendix). Thus, although the ELF in both Opt2 and Opt4 is based upon the same experimental optical data ( $q = 0$ ) and dispersion relations ( $q > 0$ ), the two constructors yield noticeable different excitation and ionization cross sections at sub-keV electron energies. The two constructors differ also on the elastic scattering model. Opt2 uses data from partial wave calculations whereas Opt4 relies on the screened Rutherford model with empirical parameters deduced specifically for water (Kyriakou *et al* 2016). Note that the dissociative attachment and vibrational excitation channels available in Opt2 were deactivated for a fair comparison between the two constructors (Opt2 and Opt4). Also, these processes are mostly effective below 10 eV which was the lowest tracking cutoff energy used in the present study.

## 2.2. Tools and methods

Microdosimetry simulations are based on the ‘microyz’ extended example of Geant4-DNA which has been described in detail elsewhere (Kyriakou *et al* 2017, Incerti *et al* 2018). Briefly, for each electron energy presented,  $10^6$  full slowing-down electron tracks are simulated in an infinite box of liquid water starting from its center. Liquid water is commonly selected as a surrogate of soft tissue since ~70% of the mammalian cells are composed of water (Cooper 2000). The primary particles were low energy electrons with initial kinetic energy of 100 eV, 200 eV, 300 eV, 500 eV, 700 eV, 1 keV, 2 keV, 5 keV, 10 keV, 20 keV, 50 keV, and 100 keV.

Simulations were carried out using tracking cutoff energies of 10 eV, 20 eV, 50 eV, and 100 eV. The tracking cut is a particularly important parameter in TS models due to the abundance of very low energy electrons as track-ends ( $<100$  eV). The latter have a very small irradiation range (~few nm) and, therefore, increase the ‘local’ energy deposition along the primary particle track. However, simulating these very low energy electrons is particularly time consuming because of the dominance of the elastic-scattering cross section below ~100 eV. The 10 eV value is a common cutoff energy in TS models of liquid water because, to a good approximation, corresponds to the ionization threshold of water in the liquid phase. It is also the low limit of application of Opt4 (see table 1). Tracking cutoff energies up to 100 eV were also examined because they correspond to the lowest limit of application of some widely-used ionization models of Geant4 (i.e. the Livermore and Penelope sets of models).

The targets examined were spheres (which facilitate achieving a uniform and isotropic irradiation) with diameter of 2.0 nm, 2.3 nm, 2.6 nm, and 3.4 nm. This particular range of diameters was chosen as representative of literature values for targets that correspond to (only) direct DNA damage. Specifically, the choice of the smallest diameter (2.0 nm) coincides with the diameter of the B-DNA helix. The 2.3 nm diameter accounts for the additional ~0.3 nm water shell around the DNA helix. The 2.6 nm diameter is a volume-equivalent to a 2.3 nm × 2.3 nm cylinder which is considered a more realistic target geometry for DNA damage studies. Finally, the choice of the largest diameter (3.4 nm) corresponds to the longest distance that a DSB is commonly specified in a straight DNA segment; i.e. 10 base pairs (bp) with bp separation equal to 0.34 nm in B-DNA helix. Within the present methodology, one may extend the size of the target volume by the diffusion range of an OH radical (e.g. typically ~5–6 nm in the cellular medium) in order to account for the additional DNA damage induced by the indirect effect (radical attack).

Simulations have been carried out with Geant4 version 10.2 (patch 01). The statistical uncertainty for the microdosimetric quantities (frequency- and dose-mean lineal energy) was below 0.1% whereas for the DNA damage yield was below 1%. These estimates were deduced from five repeated simulations (of 10<sup>6</sup> histories each) at selected energies and sphere diameters. Additional simulations have also been performed with Geant4 version 10.4 and the most recent 10.5 version. In all cases, the discrepancy among the different Geant4 versions was within the statistical uncertainty of the simulations (<1%). This was expected since no changes in the particular constructors (Opt2 and Opt4) has been documented between versions 10.2 and 10.5.

### 2.3. DNA damage methodology

In the context of classical microdosimetry the calculation of DNA damage yield follows from the stochastic energy deposition in the target volume according to the expression (Nikjoo *et al* 1991):

$$Y_i = f(\geq E_i) \times \left(\frac{N}{D}\right), \quad (1)$$

where  $E_i$  is the minimum energy required to induce the  $i$ th type of damage (hereafter called threshold energy),  $f(\geq E_i)$  is the cumulative probability distribution for energy deposited larger than  $E_i$  in the target,  $N$  is the number of targets per genome,  $D$  is the absorbed dose in the target, and  $Y_i$  is the yield of the  $i$ th type of damage per unit dose and per cell. Assuming a normal diploid cell with 6.4 Gbp cell<sup>-1</sup> and 0.34 nm/bp, then an approximate value of  $N$  may be obtained from the relation  $N(\text{cell}^{-1}) = \left(\frac{V_{\text{DNA}}}{V_{\text{target}}}\right) = \left(\frac{\pi \times (1 \text{ nm})^2 \times 6.4 \times 0.34 (\text{nm})}{\frac{4}{3} \times \pi \times (r(\text{nm}))^3}\right) 10^9$ . The absorbed dose in the spherical target equals the frequency-mean specific energy,  $z_F$ . For spherical targets a convenient relation is:

$$D(\text{Gy}) = z_F(\text{Gy}) = 0.204 \times \frac{y_F(\text{keV } \mu\text{m}^{-1})}{d(\mu\text{m})^2}, \quad (2)$$

where  $d$  is the sphere diameter and  $y_F$  is the frequency-mean lineal energy

$$y_F = \int_0^\infty y f(y) dy. \quad (3)$$

The lineal energy is defined by  $y = \varepsilon/\bar{l}$  where  $\varepsilon$  is the energy deposited in the target and  $\bar{l}$  is the mean chord length (for spherical volumes  $\bar{l} = \frac{2}{3}d$ ). Finally, the dose-mean lineal energy  $y_D$ , which is commonly used as a measure of the biological effectiveness, is calculated from

$$y_D = \int_0^\infty y d(y) dy = \frac{1}{y_F} \int_0^\infty y^2 f(y) dy. \quad (4)$$

The selection of the correct value of the threshold energy is not straightforward due to the lack of available (and conclusive) experimental data. For example, for the induction of single-strand-break (SSB) it is often assumed (based on experimental data) that  $E_{\text{SSB}} = 17.5 \text{ eV}$  (Nikjoo *et al* 2016a) or  $E_{\text{SSB}} = 10.79 \text{ eV}$  (Pater *et al* 2014) or that  $E_{\text{SSB}}$  is a linear function between 5 eV and 37.5 eV (Friedland *et al* 2011). For the induction of double-strand-break (DSB) the situation is even less clear. For example, theoretical studies have indicated that an energy of the order of ~100 eV within a ~2–3 nm sphere diameter may be sufficient for inducing a (simple) DSB (Goodhead 1989, Goodhead *et al* 1994, Hill 1999). On the other hand, experiments have indicated that electrons (or photons) with energy as low as ~10 eV can still induce DSB, possibly through a resonance mechanism (Prise *et al* 2000, Huels *et al* 2003). In the present work, the DSB threshold energy ( $E_{\text{DSB}}$ ) was deduced by a calibration procedure as follows. There is a general consensus that for low-LET radiation the total yield (direct + indirect) of DSB ranges between 30–60 DSB Gy<sup>-1</sup> cell<sup>-1</sup> (Semenenko and Stewart 2006, Wang and Rogers 2010, Nikitaki *et al* 2016, Nikjoo *et al* 2016a) with the ratio between direct and indirect effect being approximately 35:65 (Ward 1988). Estimates of the DSB yield from the MCDS version 3.10A (Stewart *et al* 2011, 2015, Stewart 2018) for

**Table 2.** Threshold energies for the induction of direct DSB for each sphere size following calibration of equation (1) to the MCDS value of  $Y_i = 17.4 \text{ DSB Gy}^{-1} \text{ cell}^{-1}$  at 100 keV electron energy.

Diameter of target sphere (nm)	$E_{\text{DSB}}$ (eV)
2.0	76
2.3	82
2.6	88
3.4	103.5

100 keV electrons ( $\sim 0.4 \text{ keV } \mu\text{m}^{-1}$ ) give a total yield of  $52.3 \text{ DSB Gy}^{-1} \text{ cell}^{-1}$  (with parameters  $\text{O}_2 = 21\%$  and  $\text{DMSO} = 0\%$ ). Then, an approximate value for the direct contribution can be obtained from MCDS by setting  $\text{O}_2 = 21\%$  and  $\text{DMSO} = 100\%$ , which yields  $17.4 \text{ DSB Gy}^{-1} \text{ cell}^{-1}$ . Note that MCDS predicts a direct-to-indirect ratio equal to 33:67, which is in good agreement with the expected ratio of 35:65 (see above). Thus, to a first approximation, the threshold energy for the induction of (direct) DSB in the present study was deduced by ‘calibration’ to the MCDS data, i.e. matching our calculated DSB yield at 100 keV to the corresponding MCDS yield ( $17.4 \text{ DSB Gy}^{-1} \text{ cell}^{-1}$ ). This calibration procedure resulted in the following threshold energies for DSB ( $E_{\text{DSB}}$ ) induction for each sphere size (see table 2). Interestingly, the  $E_{\text{DSB}}$  values of table 2 are fairly in line with the above-mentioned literature values. It should be mentioned that since the MCDS code provides data also for the indirect effect, the calibration can be extended to determine the threshold energy for the induction of DSB from the combined direct plus indirect effect, following also the proper adjustment (increase) of the target volume by several nanometers due to OH diffusion.

More recently, the development of ion-counting detectors that can simulate ionization cluster-size distributions in nanometer-sized gas volumes has offered an alternative approach to determine DNA strand break yields (Grosswendt 2004). In this approach, which is often termed nanodosimetry, the simulated energy deposition by the radiation track (which, in classical microdosimetry, is used to deduce the damage yield through equation (1)) is replaced by the measured number of ionizations. The latter is empirically correlated, through a statistical model, to the lesion probability (Garty *et al* 2006).

## 2.4. Clustered DNA damage methodology

An important aspect of DNA damage in relation to radiation quality is the degree of its complexity (Ward 1988). It is well-recognized that the more complex the DNA lesions the less likely it is to be repaired faithfully (Georgakilas *et al* 2013). To a first approximation, clustered DNA damage can be considered in the present microdosimetric approach by simply raising the threshold energy according to damage complexity. In this work, we have studied two types of clustered DNA damage (hereafter  $\text{DSB}_c$ ) which are denoted in the literature as  $\text{DSB}^+$  and  $\text{DSB}^{++}$  (Nikjoo *et al* 1997, 1999, 2001). The  $\text{DSB}^+$  represents the combination of one DSB and (at least) one SSB within 10 bp, whereas the  $\text{DSB}^{++}$  represents the combination of (at least) two DSB within 10 bp. Thus, in the present context, the scored volume for  $\text{DSB}_c$  was assumed to be a sphere of 3.4 nm diameter (in order to encompass 10 bp). The threshold energy of  $\text{DSB}^+$  is  $E_{\text{DSB}^+} = E_{\text{DSB}} + E_{\text{SSB}^*}$  with  $E_{\text{DSB}} = 103.5 \text{ eV}$  (see table 2) and  $E_{\text{SSB}^*} = 17.5 \text{ eV} \times (3.4/2.3)^3 = 56.5 \text{ eV}$  or  $E_{\text{SSB}^*} = 10.79 \text{ eV} \times (3.4/2.3)^3 = 34.8 \text{ eV}$ . The  $E_{\text{SSB}^*}$  values are obtained by scaling the SSB threshold energy (17.5 eV or 10.7 eV) associated with a sphere of 2.3 nm diameter (DNA diameter + water shell) to the target sphere of 3.4 diameter which we have here associated to the clustered DNA damage (extending up to 10 bp). On the other hand, the threshold energy of  $\text{DSB}^{++}$  is simply  $E_{\text{DSB}^{++}} = 2 \times E_{\text{DSB}} = 207$  with  $E_{\text{DSB}} = 103.5 \text{ eV}$  (see table 2).

## 3. Results and discussion

### 3.1. Lineal energy

In figure 1, we present the frequency-mean lineal energy  $y_F$  (panel (a)) and the dose-mean lineal-energy  $y_D$  (panel (b)) as a function of the electron kinetic energy over the 100 eV to 100 keV energy range for the different sphere diameters examined. The  $y_F$  ranges between  $\sim 10$ –18 ( $\text{keV } \mu\text{m}^{-1}$ ) and the  $y_D$  between  $\sim 17$ –27 ( $\text{keV } \mu\text{m}^{-1}$ ) with the maximum located at  $\sim 300 \text{ eV}$  for all spheres, in good overall agreement with the recent results of Kyriakou *et al* (2017) and Famulari *et al* (2017). Specifically, differences with Kyriakou *et al* (2017) are up to 5% for Opt2 and up to 4% for Opt4 and can be attributed to the different cutoff energies while the differences with Famulari *et al* (2017) are up to  $\sim 20\%$  and are possibly due to the different physics lists.

The dependence of  $y_F$  and  $y_D$  on the size of the spherical target, with the 2 nm diameter used as baseline, is presented in figure 2. Evidently, both quantities are quite sensitive to the size of the sphere and decrease with increasing diameter. For the sphere diameters examined in the present work, the maximum variation is  $\sim 30\%$  for  $y_F$  and  $\sim 20\%$  for  $y_D$ .

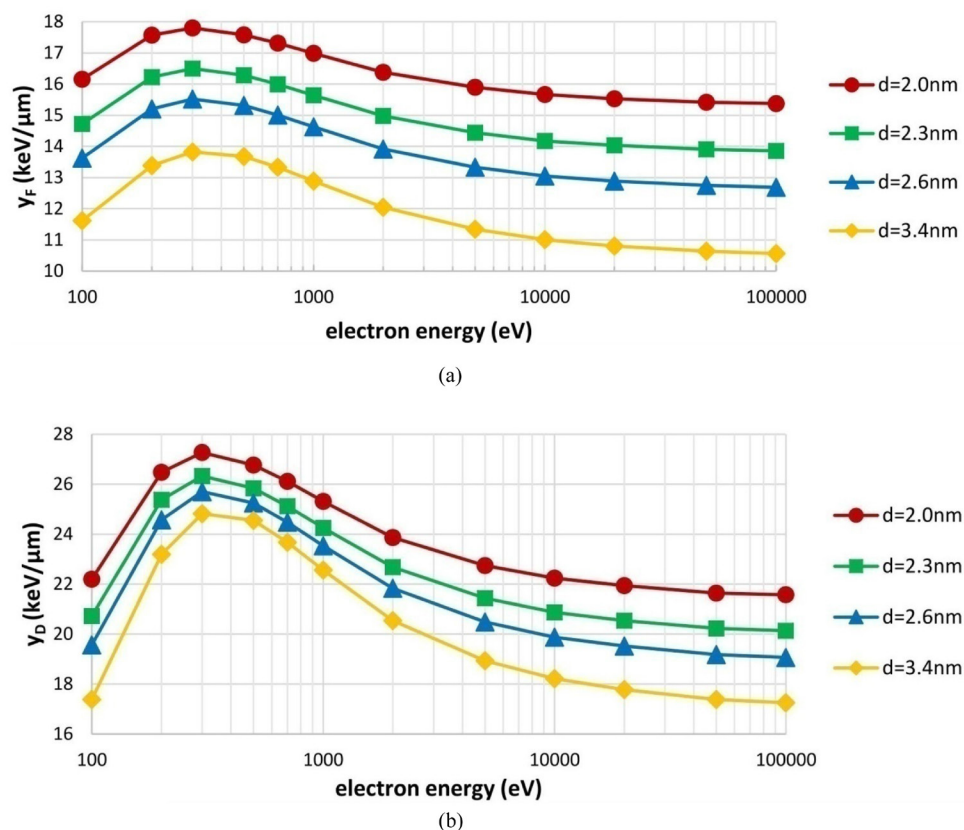


**Figure 1.** Microdosimetric quantities  $y_F$  (panel (a)) and  $y_D$  (panel (b)) as a function of the kinetic energy of the primary electron for target spheres of different diameter. The calculations are based on the Opt2 constructor (default models) of Geant4-DNA.

The influence of the physics models on  $y_F$  and  $y_D$ , with Opt2 constructor (default models) used as baseline, is shown in figure 3. Since the upper energy limit of application of Opt4 is 10 keV (see table 1), the results in figure 3 are restricted to the 100 eV–10 keV energy range. The more recent Opt4 constructor (Ioannina models) is shown to increase both  $y_F$  and  $y_D$  at all electron energies and for all sphere sizes. The difference between the physics models increases with sphere diameter and it is generally more pronounced at low than at high energies. The observed increase of lineal energy for Opt4 can be attributed to the different implementation of the dielectric function (see appendix). This leads to a different partitioning of the ELF of Opt2 and Opt4 to the ionization and excitation channels of liquid water which influences primarily the secondary electrons with very low energy (below  $\sim 50$ –100 eV), i.e. the track-ends, leading to a more localized energy deposition (Kyriakou *et al* 2015, 2016). However, overall, the effect of physics model on lineal energy remains rather small, i.e. less than 10% for  $y_F$  and 8% for  $y_D$ .

### 3.2. DSB yield

The yield of (direct) DSB as a function of the electron kinetic energy over the 100 eV to 100 keV energy range and for the different sphere sizes is presented in figure 4. For all spheres the DSB yield approaches asymptotically at high electron energies (here 100 keV) the calibration value used in the present work, i.e. 17.4 DSB Gy<sup>-1</sup> cell<sup>-1</sup> (as per MCDS). As already mentioned, the role of the calibration was to determine the threshold energy of DSB (see table 2) through equation (1). The trend of the DSB yield curve is similar for all spheres and shows a maximum value around 300 eV. The results of figure 4 reveal that the variation of the DSB yield over the low electron energy range examined (0.1–100 keV) is significant. Specifically, for the sphere sizes investigated, the yield starts at  $\sim 5$  DSB Gy<sup>-1</sup> cell<sup>-1</sup> at 100 eV, then increases rapidly to its maximum of  $\sim 40$  DSB Gy<sup>-1</sup> cell<sup>-1</sup> at 300 eV, and then falls gradually to the calibration value of 17.4 DSB Gy<sup>-1</sup> cell<sup>-1</sup> at 100 keV. That is, there is variation of a factor of 2 (or more) of the electron-induced DSB yield over the low energy range. The average initial electron energy from common x-ray imaging modalities and low-energy brachytherapy sources lies roughly between 10–100 keV. The results of figure 4 indicate that even in this limited energy range between 10–100 keV there is a 10%–12% variation of the DSB yield.

The dependence of the DSB yield on the size of the spherical target, with the 2 nm diameter used as baseline, is presented in figure 5. For most of the energy range the effect of target size appears to be modest (up to  $\sim 20\%$ ), except for the lowest energy (100 eV) where the difference increases rapidly ( $\sim 50\%$  for  $d = 2.6$  nm and  $\sim 100\%$

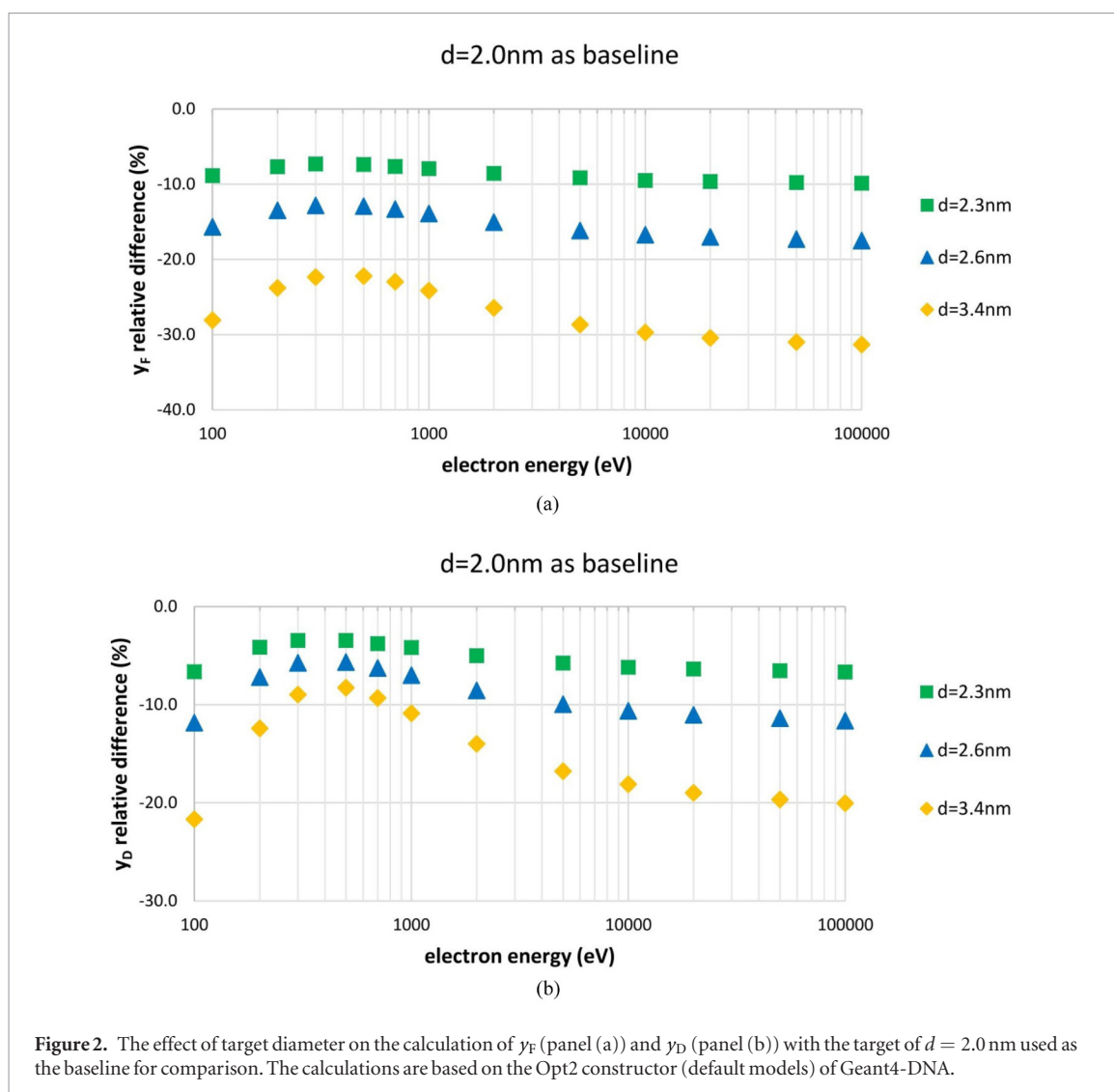


**Figure 2.** The effect of target diameter on the calculation of  $y_F$  (panel (a)) and  $y_D$  (panel (b)) with the target of  $d = 2.0\text{ nm}$  used as the baseline for comparison. The calculations are based on the Opt2 constructor (default models) of Geant4-DNA.

for  $3.4\text{ nm}$ ). The large differences for  $100\text{ eV}$  electrons are because such very low energy electrons are only marginally capable of depositing energy higher than the assumed threshold energy for DSB ( $E_{\text{DSB}}$  is between  $76\text{ eV}$  and  $103.5\text{ eV}$  for the present sphere sizes; see table 2). In particular, within the present methodology, in the case of the  $3.4\text{ nm}$  sphere, electrons with energy below (or equal to)  $100\text{ eV}$  are not capable of inducing DSB since their energy is already below the threshold of  $103.5\text{ eV}$  (see table 2). Obviously, this is a shortcoming of the threshold-energy concept, which is primarily an operational concept, since even very low energy electrons (well below the  $E_{\text{DSB}}$ ) have been found capable of inducing DSB (Huels *et al* 2003). Overall, the sensitivity of the DSB yield on the size of the target is comparable to that observed for the lineal energy ( $y_F$  and  $y_D$ ).

The influence of the physics models on the DSB yield, with Opt2 constructor (default models) used as baseline, is shown in figure 6. Since the upper energy limit of application of Opt4 is  $10\text{ keV}$ , the results in figure 6 are restricted to the  $100\text{ eV}$ – $10\text{ keV}$  energy range. The Opt4 constructor (Ioannina models) is shown to increase the DSB yield for all sphere sizes. The effect is more pronounced at low than at high energies and gradually vanishes at energies above  $10\text{ keV}$ . Similar to the case of the lineal energy (figure 3), the larger DSB yield of Opt4 compared to Opt2 can be attributed to the more localized energy deposition (i.e. shorter tracks) due to the different implementation of the dielectric function. It can be seen from figure 6 that the different DSB yield between Opt2 and Opt4 increases somewhat with sphere diameter. Overall, the effect of physics models is moderate (up to  $\sim 15\%$ ) except for the lowest energy ( $100\text{ eV}$ ) where the differences increase rapidly reaching  $17\%$  ( $d = 2\text{ nm}$ ),  $20\%$  ( $d = 2.3\text{ nm}$ ), and  $33\%$  ( $d = 2.6\text{ nm}$ ). By comparing figure 3 with 6, we can observe that the DSB yield is somewhat more sensitive to the physics model (Opt2 versus Opt4) than the lineal energy ( $y_F$  and  $y_D$ ) is.

In figure 7, we show the frequency distribution of events (tracks) with energy deposition in the target (here  $3.4\text{ nm}$  diameter sphere) above a certain value  $E$ , i.e. the distribution  $1 - f(> E)$  with  $f(> E)$  being the cumulative probability distribution of equation (1). The horizontal axis depicts only energy deposition values above  $100\text{ eV}$  since, for this particular target sphere ( $d = 3.4\text{ nm}$ ), the DSB threshold energy is  $E_{\text{DSB}} = 103.5\text{ eV}$  (see table 2). In this representation, one may clearly notice that Opt4 (Ioannina models) is more effective than Opt2

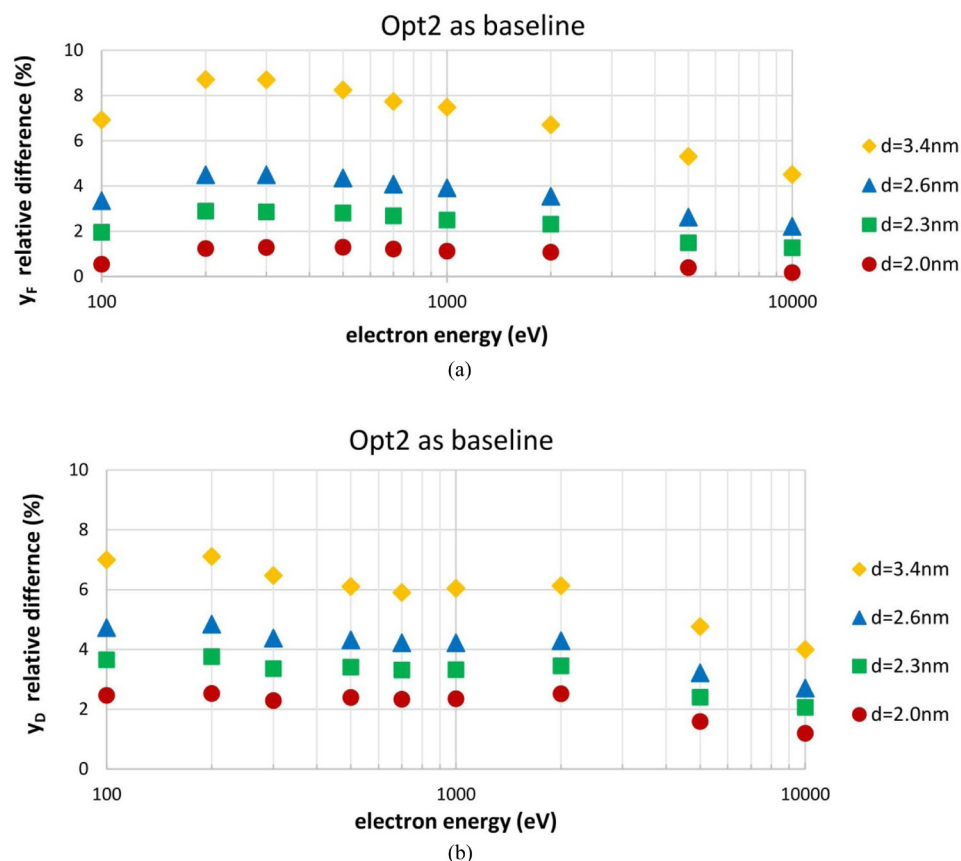


**Figure 3.** The effect of physics models on the calculation of  $\gamma_F$  (panel (a)) and  $\gamma_D$  (panel (b)) for different target diameters with the Opt2 constructor (default models) used as the baseline for comparison.

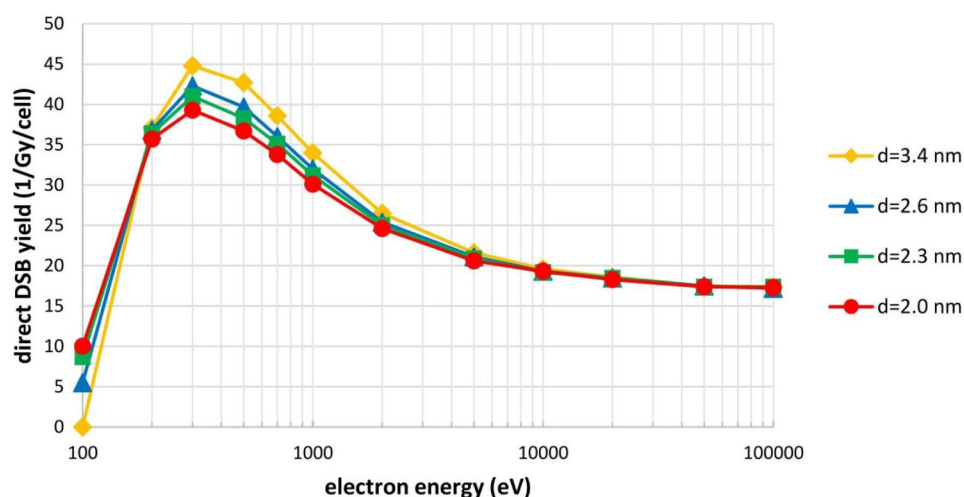
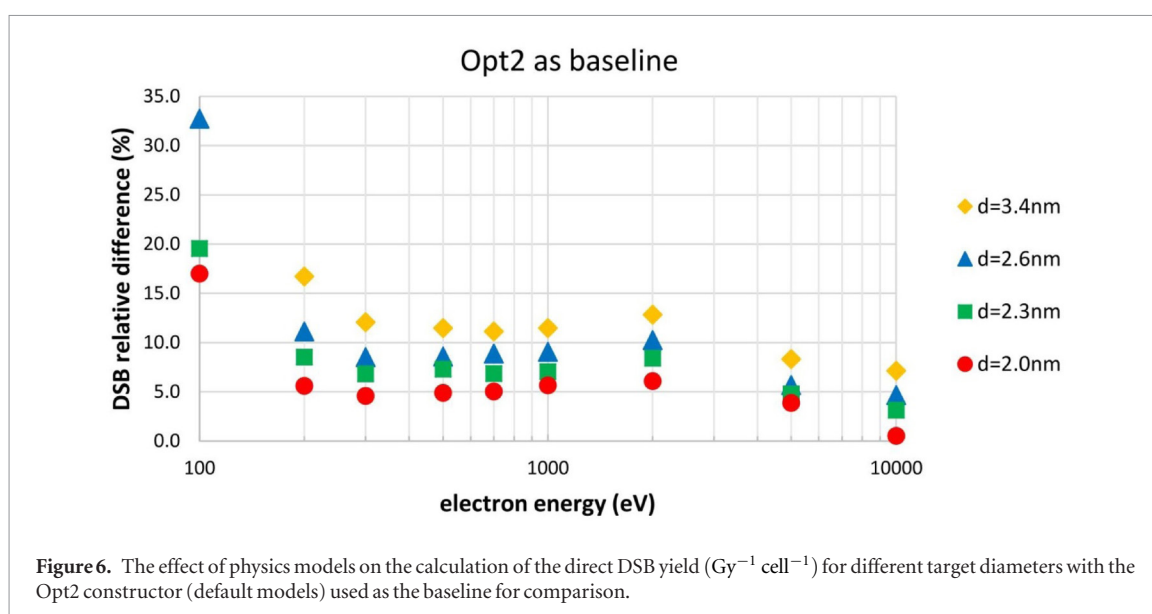
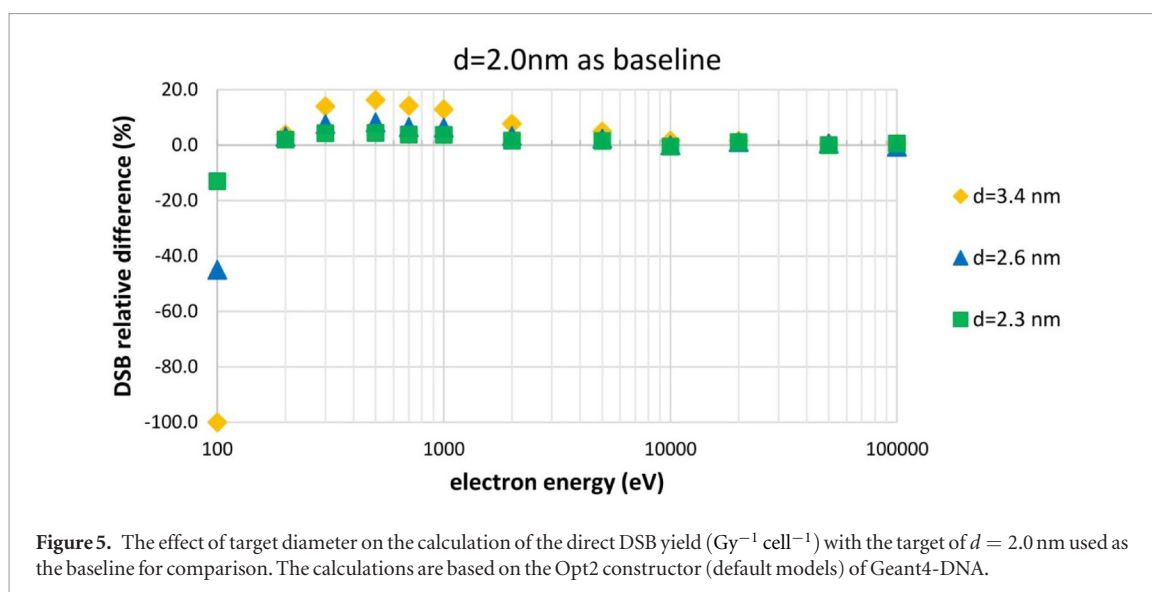


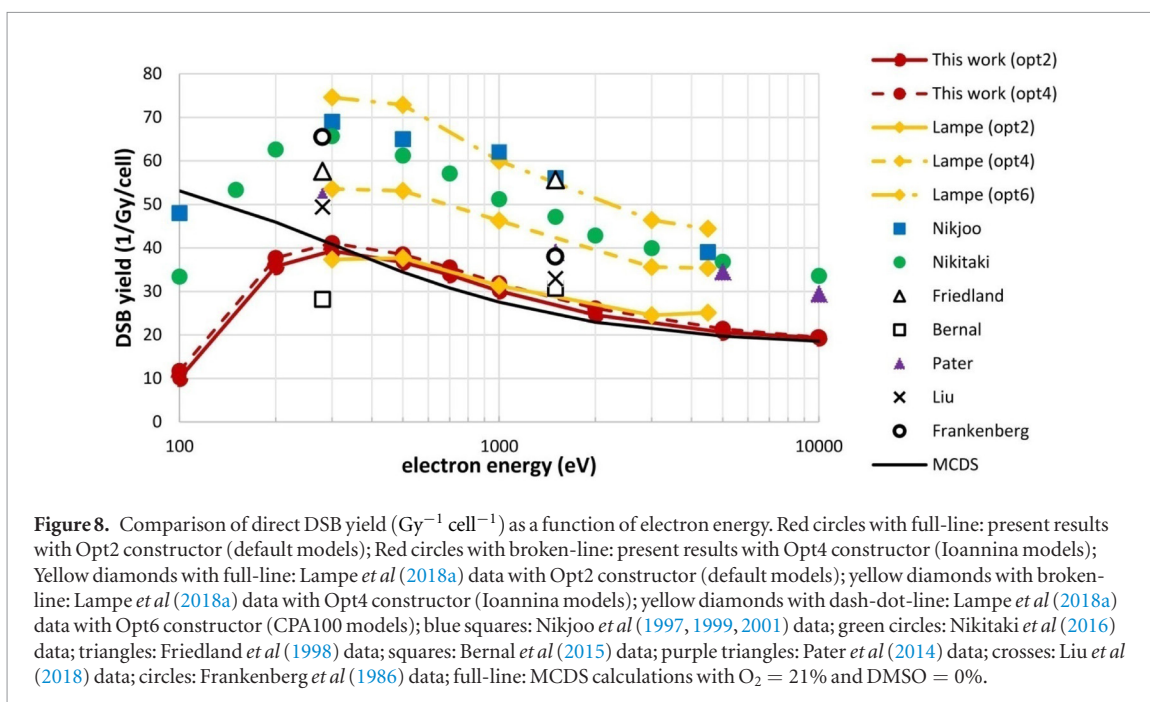
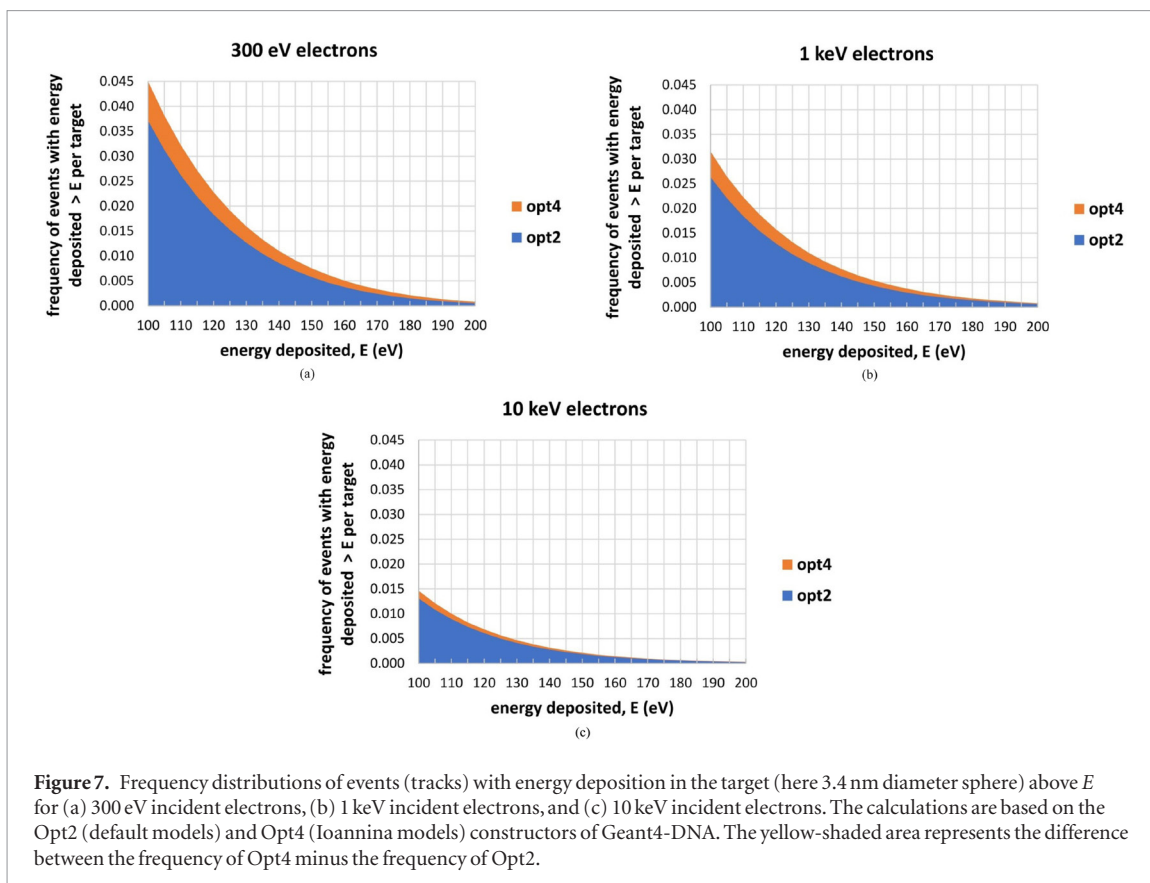
**Figure 4.** Direct DSB yield ( $\text{Gy}^{-1} \text{ cell}^{-1}$ ) as a function of the electron energy for different target diameters obtained with the Opt2 constructor (default models) of Geant4-DNA, for a total DNA length of 6.4 Gbp.

(default models) in inducing DSB because of the higher frequency of events with  $E > E_{\text{DSB}}$ . Evidently, the difference between Opt4 and Opt2 diminishes with increasing electron energy. As presented in detail elsewhere (Kyriakou *et al* 2015, 2016, 2017), the new set of models implemented in Opt4 predict less diffused electron tracks resulting in higher local energy deposition in the nanometer scale. This trend is the result of the combined effect of the excitation and elastic cross sections which are both strongly enhanced at sub-keV electron energies in Opt4 compared to Opt 2.

In figure 8, we compare the direct DSB yield calculated for the 2 nm sphere diameter using the two physics constructors (Opt2 and Opt4) against literature data. For a meaningful comparison only those studies which report *direct* DSB yields are selected from the literature. Evidently, the data from the literature have a large spread



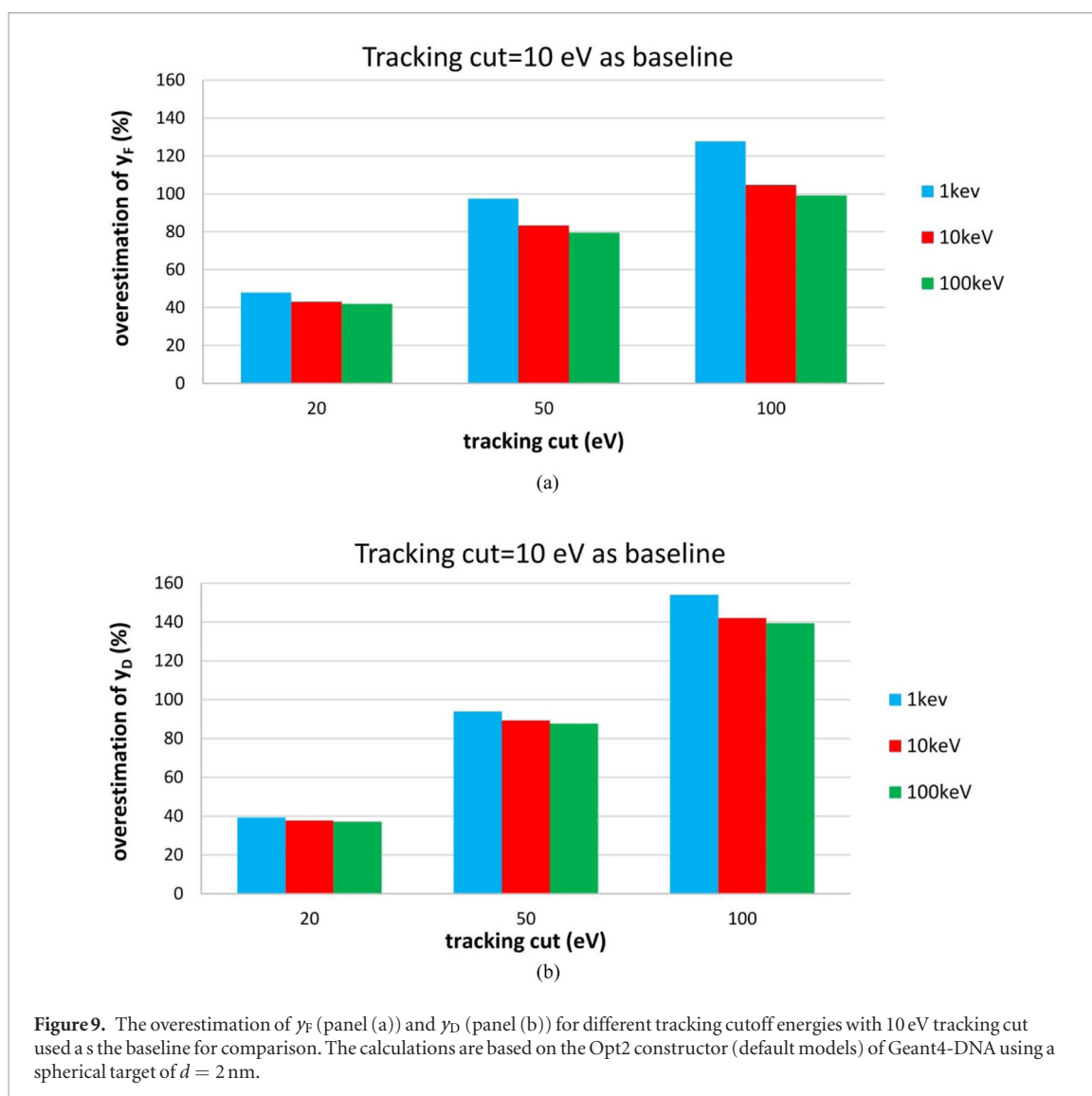
(factor of  $\sim 2$  or more) which is indicative of the large uncertainty, due to the many model assumptions and approximations, inherent in such calculations. Although most studies seem to agree on the general trend of an increased DSB yield at lower energies, the magnitude of this increase is less clear. The predictions of the present study are in good agreement with those of Lampe *et al* (2018a) only for Opt2. The Lampe *et al* study uses an atomistic model for DNA and adopts the ‘complete-chain’ approach whereby both the direct and indirect contribution are accounted for. For a meaningful comparison only the direct DSB yield of Lampe *et al* is presented in figure 8. Interestingly, the data of Lampe *et al* reveal a much higher sensitivity of the DSB yield on the physics model. Specifically, whereas our DSB yield of Opt2 is very close to the corresponding yield of Lampe *et al*, this is not the case with the DSB yield of Opt4. Specifically, Lampe *et al* predicts a significant increase ( $\sim 40\%$ ) of the direct DSB yield when switching from Opt2 to Opt4 whereas in our study the corresponding increase is much smaller (less than  $10\%$ – $15\%$ ). This observation indicates that the differences between Opt2 and Opt4 are becoming even more important in mechanistic studies. This is not surprising since the main difference between the two implementations of the dielectric function (Opt2 versus Opt4) is on the relative contribution of excitations and ionizations. Thus, the yield of chemical species is expected to be more sensitive to the choice between Opt2 and Opt4 than the energy deposition stage. Our results are also in fair agreement with those of Bernal *et al* (2015) which are based on an atomistic DNA model using the PENELOPE MC code. On the other hand, sizeable differences are observed between our study and those of Nikjoo *et al* (1997, 1999, 2001), Friedland *et al* (1998), Pater *et al* (2014) and Nikitaki *et al* (2016) which may be attributed to the use of different MC codes, physics models, and target geometries, so it is difficult to draw further conclusions. Finally, calculations are also presented for the MCDS version 3.10A (Stewart *et al* 2011) which was used for calibration in our study. As an approximation to the direct DSB yield, the parameters  $\text{O}_2 = 21\%$  and  $\text{DMSO} = 0\%$  were chosen as input to the MCDS calculations.



The agreement of our data with the MCDS results is good down to  $\sim 300$  eV with an average (absolute) difference of about 5% (Opt2) and 9% (Opt4). At even lower energies the MCDS results exhibit a monotonic increase, thus, deviating significantly from our study. In contrast to most other studies, the MCDS code does not seem to predict a peak in the energy dependence of the DSB yield (at least down to 100 eV).

### 3.3. Effect of tracking cut

All previous results have been obtained using a 10 eV tracking cutoff energy in the MC simulations, i.e. electrons with energy below this value are not further propagated and their residual energy is deposited 'at the spot'. In figure 9 we have examined the effect of tracking cut on lineal energy ( $y_F$  and  $y_D$ ) for a 2 nm sphere diameter and for electron kinetic energies of 1, 10, and 100 keV. The lineal energy data for 10 eV tracking cut are being used as

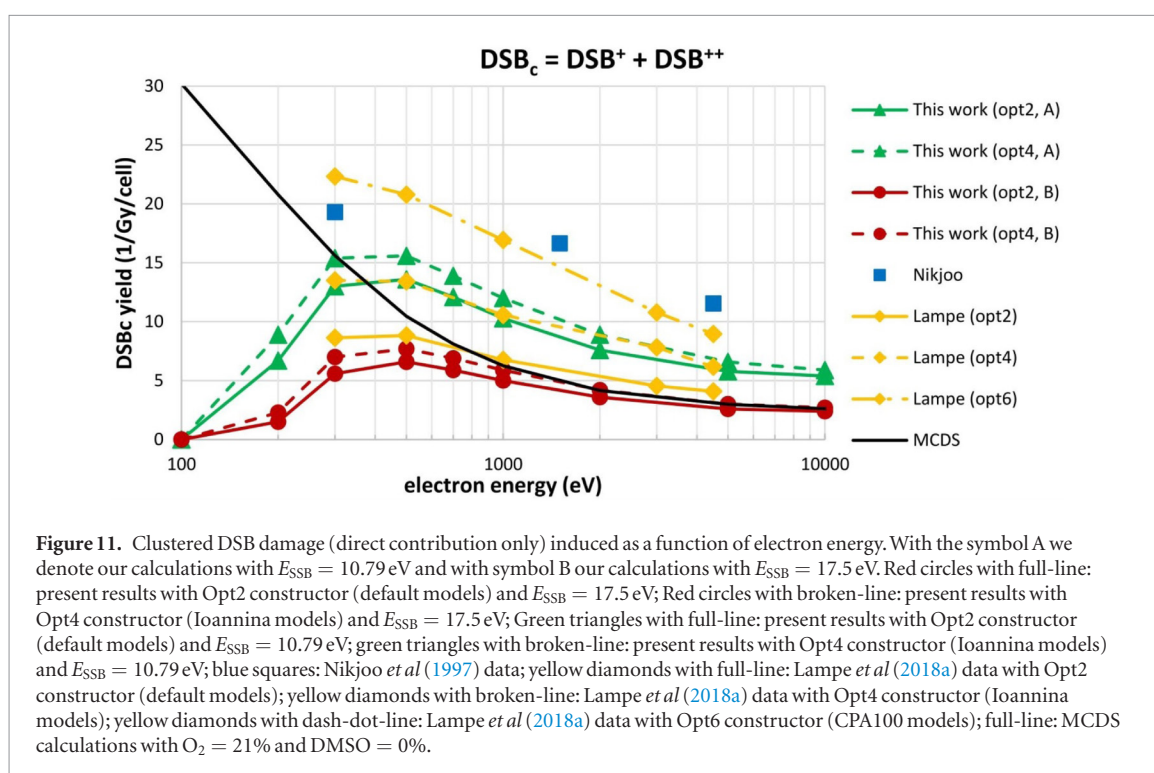
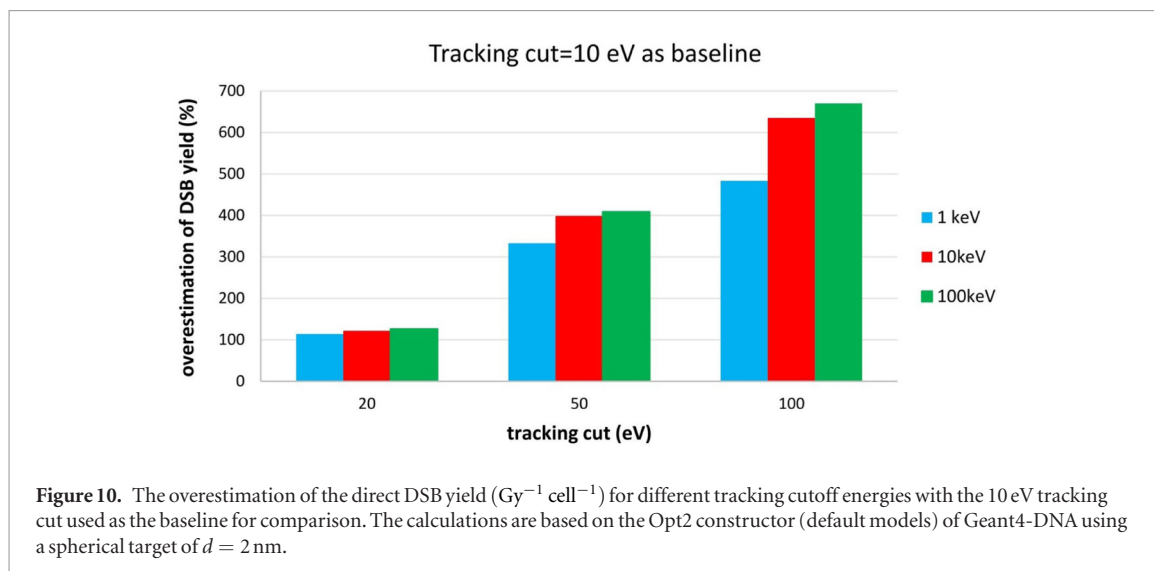


the baseline for comparison. As expected, both  $\gamma_F$  and  $\gamma_D$  increase with the tracking cutoff energy because fewer secondary electrons are given the chance to escape the target volume, thus, increasing the local energy deposition. As it can be seen, the effect of the tracking cutoff energy is significant; for example, even a small raise from 10 eV to 20 eV increases both  $\gamma_F$  and  $\gamma_D$  by  $\sim 40\%$ , while further increase to 50 eV and 100 eV increases  $\gamma_F$  by 80%–100% and  $\gamma_D$  by 100%–150%. Note that a default tracking cutoff energy of the order of 100 eV is commonly used for the low-energy EM models of Geant4 (i.e. the Livermore and Penelope models).

The effect of tracking cutoff energy on the DSB yield is shown in figure 10 for 1, 10, and 100 keV electrons. Evidently, the DSB yield is even more sensitivity to the tracking cut than it is the lineal energy ( $\gamma_F$  and  $\gamma_D$ ). For example, even a small raise of the cutoff energy from 10 eV to 20 eV increases the DSB yield by more than 100%. Interestingly, a further increase of the cutoff energy to 50 eV and 100 eV (which represent the low-energy application limits of CH models), increases the DSB yield by  $\sim 300\%$ – $400\%$  and  $\sim 500\%$ – $700\%$ , respectively. The above results clearly reveal the important role of track-ends (i.e. very low energy secondaries below  $\sim 100$  eV) in DNA damage studies and highlight the need to develop accurate physics models to describe their transport in biological media (Nikjoo *et al* 2016a). From an operational point of view, when different cutoff limits are used (i.e. higher than 10 eV), one should adjust (increase) the threshold energies accordingly in order to compensate for the enhanced DSB yields.

### 3.4. Clustered DNA damage

The yield of clustered DSB damage ( $DSB_c$ ) from the direct effect as a function of electron energy is presented in figure 11. As explained in section 2.4, in the present work we define clustered DNA damage as  $DSB_c = DSB^+ + DSB^{++}$  with  $DSB^+ = DSB + SSB$  and  $DSB^{++} = 2 \times DSB$  within 10 bp (Nikjoo *et al* 1997). For each physics model (Opt2 or Opt4) two sets of data for  $DSB_c$  are presented, corresponding to the two different threshold energies for the SSB ( $E_{SSB} = 10.79$  eV or  $E_{SSB} = 17.5$  eV). We can see from figure 11 that the  $DSB_c$  yield follows the same trend as the DSB yield (figure 4), that is, starting from high electron energies it gradually



increases with decreasing electron energy reaching a peak around 300 eV and then falls rather rapidly. In absolute values, the ratio of clustered-to-simple DSB yield calculated in our study varies in the range of  $\sim 18\%$ – $33\%$  (for  $E_{\text{SSB}} = 10.79 \text{ eV}$ ) and  $\sim 4\%$ – $16\%$  (for  $E_{\text{SSB}} = 17.5 \text{ eV}$ ) (see table 3). As expected, with increasing the threshold energy of SSB the yield of clustered DSB damage decreases (here by a factor of  $\sim 2$  or more).

In the same figure, we have also included for comparison the results of Nikjoo *et al* (1999) and Lampe *et al* (2018a), as well as results from the MCDS version 3.10A (Stewart *et al* 2011). Although there is a sizeable difference among studies, due to different physics models and/or MC codes and methodologies, the general trend of the  $\text{DSB}_c$  yield as a function of electron energy predicted by Nikjoo *et al* and Lampe *et al* is similar to our study. Interestingly, even in the more difficult case of clustered DNA damage, our results are in fair agreement with those of Lampe *et al* which use a more sophisticated mechanistic approach. As noted also in relation to the DSB yield (figure 8), the microdosimetric approach adopted in the present study is not as sensitive to the physics model (Opt2 versus Opt4) as the mechanistic approach of Lampe *et al*. The agreement of our clustered DSB yields with MCDS is not as good as in the case of simple DSB. For example, the average (absolute) difference between our  $\text{DSB}_c$  data and MCDS in the electron energy range from  $\sim 300 \text{ eV}$  to  $100 \text{ keV}$  is  $\sim 115\%$  for Opt2 and  $\sim 89\%$  for Opt4 when selecting  $E_{\text{SSB}} = 10.79 \text{ eV}$  (case A) and  $\sim 18\%$  for Opt2 and  $\sim 27\%$  for Opt4 when selecting  $E_{\text{SSB}} = 17.5 \text{ eV}$  (case B). At even lower energies the MCDS results exhibit a monotonic increase, thus, deviating even more from our study.

**Table 3.** The ratio of clustered-to-simple DSB yield per Gy per cell (expressed as percentage) for two different values of the SSB threshold energy over the examined electron energy range (100 eV–100 keV).

Physics model	$E_{SSB} = 10.79$ eV		$E_{SSB} = 17.5$ eV	
	Min (%)	Max (%)	Min (%)	Max (%)
Opt2	18.1	31.9	4.0	15.5
Opt4	20.6	32.8	5.3	16.2

## 4. Conclusion

The biological importance of the accurate calculation and prediction of complex DNA damage is currently of major importance in the field of radiation biology and radiation protection while also useful for clinical setups and the idea of radiation-induced systemic effects (Mavragani *et al* 2017). In this study a microdosimetric approach has been used to calculate the yield of direct DNA damage, in the form of simple and clustered DSB for low energy electrons. Track-structure simulations were performed with different Geant4-DNA physics models for calculating lineal energy spectra in DNA-size target volumes which were then coupled to empirical values for the threshold energy of SSB and DSB. Overall, the yield of DSB is shown to depend moderately on the physics model and target size while being particularly sensitive to the tracking cutoff energy used in the simulation. A strong dependence on electron energy for both the simple and clustered DSB yield was found which supports the notion of a variable RBE over the photon energy range used in x-ray imaging and low-energy brachytherapy. Perhaps most importantly, it is shown that a classical microdosimetry approach to DNA damage predicts comparable results to computationally intensive mechanistic approaches, thus, offering a relatively simple and robust alternative for some practical applications of radiation quality.

## Acknowledgment

We would like to acknowledge financial support from the France-Greece ‘Project International de Cooperation Scientifique (PICS)’ #8235 funded by CNRS. I Kyriakou and D Emfietzoglou acknowledge financial support from European Space Agency (ESA Contract No. 4000126645/19/NL/BW).

## Appendix

The calculation of inelastic cross sections for non-relativistic electrons by the Opt2 and Opt4 constructors of Geant4-DNA is based on the following expression of the first Born approximation (Nikjoo *et al* 2016a):

$$\frac{d^2\sigma_{\text{Born}}}{dE dq} = \frac{1}{\pi a_0 N T} \frac{1}{q} \left\{ \frac{\text{Im}[\varepsilon(E, q)]}{\text{Re}[\varepsilon(E, q)]^2 + \text{Im}[\varepsilon(E, q)]^2} \right\}, \quad (\text{A.1})$$

where  $a_0$  is the Bohr radius,  $T$  is the electron kinetic energy,  $N$  is the density of target centers (here water molecules),  $E$  is the energy-transfer,  $q$  is the momentum-transfer,  $\varepsilon(E, q)$  is the dielectric function, and  $\text{Im}[-1/\varepsilon(E, q)] = \text{Im}[\varepsilon(E, q)] / \{\text{Re}[\varepsilon(E, q)]^2 + \text{Im}[\varepsilon(E, q)]^2\}$  is the ELF. Integration of equation (A.1) over  $q$  gives the differential energy-loss cross sections, and a subsequent integration over  $E$  gives inverse inelastic mean free paths ( $= N\sigma$ ). In Opt2 the imaginary part of the dielectric function at the optical limit (equivalent to the photoabsorption spectrum) is partitioned to the individual ionization shells and excitation levels according to Kyriakou *et al* (2015, 2016):

$$\begin{aligned} \text{Im}[\varepsilon(E, q=0)]_{\text{Opt2}} &= \sum_n^{\text{ioniz.}} \text{Im}[\varepsilon_n(E, q=0)] + \sum_k^{\text{excit.}} \text{Im}[\varepsilon_k(E, q=0)] \\ &= \sum_n^{\text{ioniz.}} [D_n(E; E_n)\Theta(E - B_n)] + \sum_k^{\text{excit.}} [D_k^*(E; E_k)\Theta(E - B_k)], \end{aligned} \quad (\text{A.2})$$

where  $D_n(E; E_n)$  and  $D_k^*(E; E_k)$  are ionization and excitation Drude functions, respectively, and  $B_{n,k}$  are threshold energies (e.g. binding energies for ionization shells). However, as discussed elsewhere (Kyriakou *et al* 2015, 2016), the implementation of equation (A.2) results in partial violation of the f-sum-rule and an incorrect calculation of the real part of the dielectric function,  $\text{Re}[\varepsilon(E, q=0)]$ , through the Kramers-Kronig relation. The above deficiencies are overcome in Opt4 by replacing equation (A.2) by the expression (Kyriakou *et al* 2015, 2016):

$$\begin{aligned}
\text{Im}[\varepsilon(E, q=0)]_{\text{Opt4}} &= \sum_n^{\text{ioniz.}} \text{Im}[\varepsilon_n(E, q=0)] + \sum_k^{\text{excit.}} \text{Im}[\varepsilon_k(E, q=0)] \\
&= \sum_n^{\text{ioniz.}} \{[D_n(E; E_n) - D_n(E; B_n) \exp(B_n - E) + F_n(E)]\Theta(E - B_n)\} \\
&\quad + \sum_k^{\text{excit.}} \{[D_k^*(E; E_k) + F_k(E)]\Theta(E - B_k)\},
\end{aligned} \tag{A.3}$$

where  $D_n(E; B_n) \exp(B_n - E)$  is an exponential smoothing function for ionisations, and  $F_{n,k}(E)$  are contributions due to the truncation of the ionization Drude functions at the corresponding threshold energies. Despite starting from essentially the same optical data for  $\varepsilon(E, q=0)$ , the ELF's resulting from equation (A.2) (used in Opt2) and equation (A.3) (used in Opt4) yield substantially different ionisation and excitation cross sections calculated by equation (A.1). In particular, since  $F_{n,k}(E)$  are positive-value functions, equation (A.3) leads to an increased contribution of the excitation channels relative to ionizations (Kyriakou et al 2015, 2016).

## ORCID iDs

Ioanna Kyriakou  <https://orcid.org/0000-0003-2105-4078>  
 Alexandros G Georgakilas  <https://orcid.org/0000-0002-5971-0010>  
 Sebastien Incerti  <https://orcid.org/0000-0002-0619-2053>  
 Dimitris Emfietzoglou  <https://orcid.org/0000-0002-9996-797X>

## References

- Agostinelli S et al 2003 Geant4—a simulation toolkit *Nucl. Instrum. Methods Phys. Res. A* **506** 250–303
- Allison J et al 2006 Geant4 developments and applications *IEEE Trans. Nucl. Sci.* **53** 270–8
- Allison J et al 2016 Recent developments in Geant 4 *Nucl. Instrum. Methods Phys. Res. A* **835** 186–225
- Alloni D, Campa A, Friedland W, Mariotti L and Ottolenghi A 2012 Track structure, radiation quality and initial radiobiological events: Considerations based on the PARTRAC code experience *Int. J. Radiat. Biol.* **88** 77–86
- Andreo P 1991 Monte Carlo techniques in medical radiation physics *Phys. Med. Biol.* **36** 861–920
- Baró J, Sempau J, Fernández-Varea J M and Salvat F 1995 PENELOPE: An algorithm for Monte Carlo simulation of the penetration and energy loss of electrons and positrons in matter *Nucl. Instrum. Methods Phys. Res. B* **100** 31–46
- Bernal M A et al 2015 Track structure modeling in liquid water: A review of the Geant4-DNA very low energy extension of the Geant4 Monte Carlo simulation toolkit *Phys. Medica* **31** 861–74
- Bernal M A and Liendo J A 2009 An investigation on the capabilities of the PENELOPE MC code in nanodosimetry: PENELOPE code in nanodosimetry *Med. Phys.* **36** 620–5
- Bopp C, Hirayama R, Inaniwa T, Kitagawa A, Matsufuji N and Noda K 2016 Adaptation of the microdosimetric kinetic model to hypoxia *Phys. Med. Biol.* **61** 7586–99
- Bordage M C, Bordes J, Edel S, Terrissol M, Franceries X, Bardiès M, Lampe N and Incerti S 2016 Implementation of new physics models for low energy electrons in liquid water in Geant4-DNA *Phys. Medica* **32** 1833–40
- Champion C 2003 Theoretical cross sections for electron collisions in water: structure of electron tracks *Phys. Med. Biol.* **48** 2147–68
- Chatzipapas K P, Papadimitroulas P, Obeidat M, McConnell K A, Kirby N, Loudos G, Papanikolaou N and Kagadis G C 2019 Quantification of DNA double strand breaks using Geant4-DNA *Med. Phys.* **46** 405–13
- Cooper G M 2000 *The Cell: A Molecular Approach* (Washington, DC: ASM Press)
- Dingfelder M 2006 Track structure: time evolution from physics to chemistry *Radiat. Prot. Dosim.* **122** 16–21
- Dingfelder M 2012 Track-structure simulations for charged particles *Health Phys.* **103** 590–5
- Dingfelder M, Hantke D, Inokuti M and Paretzke H G 1998 Electron inelastic-scattering cross sections in liquid water *Radiat. Phys. Chem.* **53** 1–18
- Dingfelder M, Ritchie R H, Turner J E, Friedland W, Paretzke H G and Hamm R N 2008 Comparisons of calculations with PARTRAC and NOREC: transport of electrons in liquid water *Radiat. Res.* **169** 584–94
- El Naqa I, Pater P and Seuntjens J 2012 Monte Carlo role in radiobiological modelling of radiotherapy outcomes *Phys. Med. Biol.* **57** R75–97
- Emfietzoglou D and Nikjoo H 2005 The effect of model approximations on single-collision distributions of low-energy electrons in liquid water *Radiat. Res.* **163** 98–111
- Emfietzoglou D and Nikjoo H 2007 Accurate electron inelastic cross sections and stopping powers for liquid water over the 0.1–10 keV range based on an improved dielectric description of the Bethe surface *Radiat. Res.* **167** 110–20
- Emfietzoglou D, Kyriakou I, Abril I, Garcia-Molina R and Nikjoo H 2012 Inelastic scattering of low-energy electrons in liquid water computed from optical-data models of the Bethe surface *Int. J. Radiat. Biol.* **88** 22–8
- Emfietzoglou D, Kyriakou I, Garcia-Molina R and Abril I 2017a Inelastic mean free path of low-energy electrons in condensed media: beyond the standard models: low-energy electron inelastic mean free paths *Surf. Interface Anal.* **49** 4–10
- Emfietzoglou D, Papamichael G and Nikjoo H 2017b Monte Carlo electron track structure calculations in liquid water using a new model dielectric response function *Radiat. Res.* **188** 355–68
- Falk M, af Rosenschöld P M, Keall P, Cattell H, Cho B C, Poulsen P, Povzner S, Sawant A, Zimmerman J and Korreman S 2010 Real-time dynamic MLC tracking for inversely optimized arc radiotherapy *Radiother. Oncol.* **94** 218–23
- Famulari G, Pater P and Enger S A 2018 Microdosimetric evaluation of current and alternative brachytherapy sources—a Geant4-DNA simulation study *Int. J. Radiat. Oncol. Biol. Phys.* **100** 270–7
- Famulari G, Pater P and Enger S A 2017 Microdosimetry calculations for monoenergetic electrons using Geant4-DNA combined with a weighted track sampling algorithm *Phys. Med. Biol.* **62** 5495–508
- Ferrari A, Sala P R, Fasso A and Ranft J 2005 *FLUKA: a Multi-Particle Transport Code* (Geneva: CERN) ([www.osti.gov/servlets/purl/877507-sC9S9L/](http://www.osti.gov/servlets/purl/877507-sC9S9L/))

- Frankenberg D, Goodhead D T, Frankenberg-Schwager M, Harbich R, Bance D A and Wilkinson R E 1986 Effectiveness of 1.5 keV aluminium K and 0.3 carbon K characteristic x-rays at inducing DNA double-strand breaks in yeast cells *Int. J. Radiat. Biol.* **50** 727–41
- Friedland W, Dingfelder M, Kunderát P and Jacob P 2011 Track structures, DNA targets and radiation effects in the biophysical Monte Carlo simulation code PARTRAC *Mutation Res./Fundam. Mol. Mech. Mutagen.* **711** 28–40
- Friedland W, Paretzke H G, Ballarini F, Ottolenghi A, Kreth G and Cremer C 2008 First steps towards systems radiation biology studies concerned with DNA and chromosome structure within living cells *Radiat. Environ. Biophys.* **47** 49–61
- Friedland W, Schmitt E, Kunderát P, Dingfelder M, Baiocco G, Barbieri S and Ottolenghi A 2017 Comprehensive track-structure based evaluation of DNA damage by light ions from radiotherapy-relevant energies down to stopping *Sci. Rep.* **7** 45161
- Friedland W, Jacob P, Paretzke H G and Stork T 1998 Monte Carlo simulation of the production of short DNA fragments by low-linear energy transfer radiation using high-order DNA molecules *Radiat. Res.* **150** 170–82
- Garcia-Molina R, Abril I, Kyriakou I and Emfietzoglou D 2017 Inelastic scattering and energy loss of swift electron beams in biologically relevant materials: energy loss of electron beams in biomaterials *Surf. Interface Anal.* **49** 11–7
- Garty G, Schulte R, Shchemelinin S, Grosswendt B, Leloup C, Assaf G, Breskin A, Chechik R and Bashkirov V 2006 First attempt at prediction of DNA strand-break yields using nanodosimetric data *Radiat. Prot. Dosim.* **122** 451–4
- Georgakilas A G, O'Neill P and Stewart R D 2013 Induction and repair of clustered DNA lesions: what do we know so far? *Radiat. Res.* **180** 100–9
- Goodhead D T 1989 The initial physical damage produced by ionizing radiations *Int. J. Radiat. Biol.* **56** 623–34
- Goodhead D T, Leenhouts H P, Paretzke H G, Terrissol M, Nikjoo H and Blaauboer R 1994 Track structure approaches to the interpretation of radiation effects on DNA *Radiat. Prot. Dosim.* **52** 217–23
- Goorley T et al 2016 Features of MCNP6 *Ann. Nucl. Energy* **87** 772–83
- Grosswendt B 2004 Recent advances of nanodosimetry *Radiat. Prot. Dosim.* **110** 845–50
- Henthorn N T, Warmenhoven J W, Sotiropoulos M, Mackay R I, Kirkby N F, Kirkby K J and Merchant M J 2018 In silico non-homologous end joining following ion induced DNA double strand breaks predicts that repair fidelity depends on break density *Sci. Rep.* **8** 2654
- Hill M A 1999 Radiation damage to DNA: the importance of track structure *Radiat. Meas.* **31** 15–23
- Huels M A, Boudaïffa B, Cloutier P, Hunting D and Sanche L 2003 Single, double, and multiple double strand breaks induced in DNA by 3 – 100 eV electrons *J. Am. Chem. Soc.* **125** 4467–77
- ICRU 36 1983 Microdosimetry *J. Int. Comm. Radiat. Units Meas.* **os19**
- ICRU 40 1986 The quality factor in radiation protection *J. Int. Comm. Radiat. Units Meas.* **os21**
- Inaniwa T, Furukawa T, Kase Y, Matsufuji N, Toshito T, Matsumoto Y, Furusawa Y and Noda K 2010 Treatment planning for a scanned carbon beam with a modified microdosimetric kinetic model *Phys. Med. Biol.* **55** 6721–37
- Incerti S, Douglass M, Penfold S, Guatelli S and Bezak E 2016 Review of Geant4-DNA applications for micro and nanoscale simulations *Phys. Medica* **32** 1187–200
- Incerti S et al 2010a The Geant4-DNA project *Int. J. Model. Simulat. Sci. Comput.* **1** 157–78
- Incerti S et al 2010b Comparison of GEANT4 very low energy cross section models with experimental data in water *Med. Phys.* **37** 4692–708
- Incerti S et al 2018 Geant4-DNA example applications for track structure simulations in liquid water: A report from the Geant4-DNA Project *Med. Phys.* **45** e722–39
- Incerti S, Kyriakou I, Bordage M C, Guatelli S, Ivanchenko V and Emfietzoglou D 2019 Track structure simulations of proximity functions in liquid water using the Geant4-DNA toolkit *J. Appl. Phys.* **125** 104301
- Ingram S P, Warmenhoven J W, Henthorn N T, Smith E A K, Chadwick A L, Burnet N G, Mackay R I, Kirkby N F, Kirkby K J and Merchant M J 2019 Mechanistic modelling supports entwined rather than exclusively competitive DNA double-strand break repair pathway *Sci. Rep.* **9** 6359
- Kawrakow I 2000 Accurate condensed history Monte Carlo simulation of electron transport. I. EGS nrc, the new EGS4 version *Med. Phys.* **27** 485–98
- Kellerer A M and Rossi H H 1978 A generalized formulation of dual radiation action *Radiat. Res.* **75** 471
- Kellerer A M and Rossi H H 1974 The theory of dual radiation action *Curr. Topics Radiat. Res.* **8** 85–158
- Kyriakou I, Emfietzoglou D, Ivanchenko V, Bordage M C, Guatelli S, Lazarakis P, Tran H N and Incerti S 2017 Microdosimetry of electrons in liquid water using the low-energy models of Geant4 *J. Appl. Phys.* **122** 024303
- Kyriakou I, Incerti S and Francis Z 2015 Technical Note: Improvements in geant 4 energy-loss model and the effect on low-energy electron transport in liquid water: Low-energy electron energy-loss model *Med. Phys.* **42** 3870–6
- Kyriakou I, Ivanchenko V, Sakata D, Bordage M C, Guatelli S, Incerti S and Emfietzoglou D 2019 Influence of track structure and condensed history physics models of Geant4 to nanoscale electron transport in liquid water *Phys. Medica* **58** 149–54
- Kyriakou I, Šefl M, Nourry V and Incerti S 2016 The impact of new Geant4-DNA cross section models on electron track structure simulations in liquid water *J. Appl. Phys.* **119** 194902
- Lampe N, Karamitros M, Breton V, Brown J M C, Kyriakou I, Sakata D, Sarramia D and Incerti S 2018a Mechanistic DNA damage simulations in Geant4-DNA part 1: a parameter study in a simplified geometry *Phys. Medica* **48** 135–45
- Lampe N, Karamitros M, Breton V, Brown J M C, Sakata D, Sarramia D and Incerti S 2018b Mechanistic DNA damage simulations in Geant4-DNA Part 2: electron and proton damage in a bacterial cell *Phys. Medica* **48** 146–55
- Lazarakis P, Incerti S, Ivanchenko V, Kyriakou I, Emfietzoglou D, Corde S, Rosenfeld A B, Lerch M, Tehei M and Guatelli S 2018 Investigation of track structure and condensed history physics models for applications in radiation dosimetry on a micro and nano scale in Geant4 *BioMed. Phys. Eng. Express* **4** 024001
- Liamsuwan T, Emfietzoglou D, Uehara S and Nikjoo H 2012 Microdosimetry of low-energy electrons *Int. J. Radiat. Biol.* **88** 899–907
- Liljequist D and Nikjoo H 2014 On the validity of the trajectory methods for calculating the transport of very low energy (<1 keV) electrons in liquids and amorphous media *Radiat. Phys. Chem.* **99** 45–52
- Lindborg L, Hultqvist M, Carlsson Tedgren Å and Nikjoo H 2013 Lineal energy and radiation quality in radiation therapy: model calculations and comparison with experiment *Phys. Med. Biol.* **58** 3089–105
- Lindborg L and Nikjoo H 2011 Microdosimetry and radiation quality determinations in radiation protection and radiation therapy *Radiat. Prot. Dosim.* **143** 402–8
- Lindborg L and Grindborg J-E 1997 Nanodosimetric results and radiotherapy beams: a clinical application? *Radiat. Prot. Dosim.* **1–4** 541–6
- Liu W, Tan Z, Zhang L and Champion C 2018 Investigation on the correlation between energy deposition and clustered DNA damage induced by low-energy electrons *Radiat. Environ. Biophys.* **57** 179–87
- Meylan S, Incerti S, Karamitros M, Tang N, Bueno M, Clairard I and Villagrana C 2017 Simulation of early DNA damage after the irradiation of a fibroblast cell nucleus using Geant4-DNA *Sci. Rep.* **7** 11923
- Mavragani I, Nikitaki Z, Souli M, Aziz A, Newsheer S, Aziz K, Rogakou E and Georgakilas A 2017 Complex DNA damage: a route to radiation-induced genomic instability and carcinogenesis *Cancers* **9** 91

- McNamara A, Geng C, Turner R, Ramos-Mendez J, Perl J, Held K, Faddegon B, Paganetti H and Schuemann J 2017 Validation of the radiobiology toolkit TOPAS-nBio in simple DNA geometries *Phys. Medica* **33** 207–15
- McNamara A et al 2018 Geometrical structures for radiation biology research as implemented in TOPAS-nBio toolkit *Phys. Med. Biol.* **63** 175018
- Nahum A E 1999 Condensed-history Monte-Carlo simulation for charged particles: what can it do for us? *Radiat. Environ. Biophys.* **38** 163–73
- Nikitaki Z et al 2016 Measurement of complex DNA damage induction and repair in human cellular systems after exposure to ionizing radiations of varying linear energy transfer (LET) *Free Radical Res.* **50** S64–78
- Nikjoo H, Emfietzoglou D, Liamsuwan T, Taleei R, Liljequist D and Uehara S 2016a Radiation track, DNA damage and response—a review *Rep. Prog. Phys.* **79** 116601
- Nikjoo H, Taleei R, Liamsuwan T, Liljequist D and Emfietzoglou D 2016b Perspectives in radiation biophysics: from radiation track structure simulation to mechanistic models of DNA damage and repair *Radiat. Phys. Chem.* **128** 3–10
- Nikjoo H and Girard P 2012 A model of the cell nucleus for DNA damage calculations *Int. J. Radiat. Biol.* **88** 87–97
- Nikjoo H, Goorley T, Fulford J, Takakura K and Ito T 2002 Quantitative analysis of energetics of DNA damage *Radiat. Prot. Dosim.* **99** 91–8
- Nikjoo H and Lindborg L 2010 RBE of low energy electrons and photons *Phys. Med. Biol.* **55** R65–109
- Nikjoo H, O'Neill P, Terrissol M and Goodhead D T 1999 Quantitative modelling of DNA damage using Monte Carlo track structure method *Radiat. Environ. Biophys.* **38** 31–8
- Nikjoo H, O'Neill P, Wilson W E and Goodhead D T 2001 Computational approach for determining the spectrum of DNA damage induced by ionizing radiation *Radiat. Res.* **156** 577–83
- Nikjoo H, Uehara S, Emfietzoglou D and Cucinotta F A 2006 Track-structure codes in radiation research *Radiat. Meas.* **41** 1052–74
- Nikjoo H, Uehara S, Emfietzoglou D and Pinsky L 2011 A database of frequency distributions of energy depositions in small-size targets by electrons and ions *Radiat. Prot. Dosim.* **143** 145–51
- Nikjoo H, O'Neill P and Goodhead D T 1997 Computational modelling of low-energy electron-induced DNA damage by early physical and chemical events *Int. J. Radiat. Biol.* **71** 467–83
- Nikjoo H, Goodhead D T, Charlton D E and Paretzke H G 1991 Energy deposition in small cylindrical targets by monoenergetic electrons *Int. J. Radiat. Biol.* **60** 739–56
- Pater P, Seuntjens J, El Naqa I and Bernal M A 2014 On the consistency of Monte Carlo track structure DNA damage simulations: consistency of MCTS DNA damage simulations *Med. Phys.* **41** 121708
- Prise K M, Folkard M, Michael B D, Vojnovic B, Brocklehurst B, Hopkirk A and Munro I H 2000 Critical energies for SSB and DSB induction in plasmid DNA by low-energy photons: action spectra for strand-break induction in plasmid DNA irradiated in vacuum *Int. J. Radiat. Biol.* **76** 881–90
- Ramos-Mendez J, Perl J, Schuemann J, McNamara A, Paganetti H and Faddegon B 2018 Monte Carlo simulation of chemistry following radiolysis with TOPAS-nBio *Phys. Med. Biol.* **63** 105014
- Rossi H H and Zaider M 1996 *Microdosimetry and Its Applications* (Berlin: Springer)
- Sakata D et al 2019 Evaluation of early radiation DNA damage in a fractal cell nucleus model using Geant4-DNA *Phys. Medica* **62** 152–7
- Salvat F and Fernández-Varea J M 2009 Overview of physical interaction models for photon and electron transport used in Monte Carlo codes *Metrologia* **46** S112–38
- Schuemann J, McNamara A L, Ramos-Méndez J, Perl J, Held K D, Paganetti H, Incerti S and Faddegon B 2019a TOPAS-nBio: an extension to the TOPAS simulation toolkit for cellular and sub-cellular radiobiology *Radiat. Res.* **191** 125
- Schuemann J et al 2019b A new standard DNA damage (SDD) data format *Radiat. Res.* **191** 76
- Semenenko V A and Stewart R D 2004 A Fast Monte Carlo Algorithm to simulate the spectrum of DNA damages formed by ionizing radiation *Radiat. Res.* **161** 451–7
- Semenenko V A and Stewart R D 2006 Fast Monte Carlo simulation of DNA damage formed by electrons and light ions *Phys. Med. Biol.* **51** 1693–706
- Stewart R D, Yu V K, Georgakilas A G, Koumenis C, Park J H and Carlson D J 2011 Effects of radiation quality and oxygen on clustered DNA lesions and cell death *Radiat. Res.* **176** 587–602
- Stewart R D, Streitmatter S W, Argento D C, Kirkby C, Goorley J T, Moffitt G, Jevremovic T and Sandison G A 2015 Rapid MCNP simulation of DNA double strand break (DSB) relative biological effectiveness (RBE) for photons, neutrons, and light ions *Phys. Med. Biol.* **60** 8249–74
- Stewart R D, Carlson D J, Butkus M P, Hawkins R, Friedrich T and Scholz M 2018 A comparison of mechanism-inspired models for particle relative biological effectiveness (RBE) *Med. Phys.* **45** e925–52
- Stewart R D 2018 Induction of DNA damage by light ions relative to  $^{60}\text{Co}$  gamma-rays *Int. J. Part. Ther.* **5** 25–39
- Streitmatter S W, Stewart R D, Jenkins P A and Jevremovic T 2017 DNA double strand break (DSB) induction and cell survival in iodine-enhanced computed tomography (CT) *Phys. Med. Biol.* **62** 6164–84
- Taleei R and Nikjoo H 2012 Repair of the double-strand breaks induced by low energy electrons: a modelling approach *Int. J. Radiat. Biol.* **88** 948–53
- Taschereau R, Roy R and Pouliot J 2003 A comparison of methods to calculate biological effectiveness (RBE) from Monte Carlo simulations *Med. Dosim.* **28** 21–6
- Thomson R M and Kawrakow I 2018 Quantum versus classical Monte Carlo simulation of low-energy electron transport in condensed amorphous media *Phys. Medica* **54** 179–88
- Thomson R M and Kawrakow I 2011 On the Monte Carlo simulation of electron transport in the sub-1 keV energy range *Med. Phys.* **38** 4531–4
- Villagrasa C, Bordage M-C, Bueno M, Bug M, Chiriotti S, Gargioni E, Heide B, Nettelbeck H, Parisi A and Rabus H 2019 Assessing the contribution of cross sections to the uncertainty of Monte Carlo calculations in micro- and nanodosimetry *Radiat. Prot. Dosim.* **183** 11–6
- Wang L L W and Rogers D W O 2010 Replacement correction factors for plane-parallel ion chambers in electron beams: replacement correction factors plane-parallel chambers in electron beams *Med. Phys.* **37** 461–5
- Ward J F 1988 DNA damage produced by ionizing radiation in mammalian cells: identities, mechanisms of formation, and reparability *Prog. Nucleic Acid Res. Mol. Biol.* **35** 95–125
- Wuu C S, Kliauga P and Amols H I 1996 Microdosimetric evaluation of relative biological effectiveness for  $^{103}\text{Pd}$ ,  $^{125}\text{I}$ ,  $^{241}\text{Am}$ , and  $^{192}\text{Ir}$  brachytherapy sources *Int. J. Radiat. Oncol. Biol. Phys.* **36** 689–97
- Wuu C S and Zaider M 1998 A calculation of the relative biological effectiveness of  $^{125}\text{I}$  and  $^{103}\text{Pd}$  brachytherapy sources using the concept of proximity function *Med. Phys.* **25** 2186–9
- Zaider M, Bardash M and Fung A 1994 Molecular damage induced directly and indirectly by ionizing radiation in DNA *Int. J. Radiat. Biol.* **66** 459–65